Does higher spatial resolution improve snow estimates?

Edward H. Bair[1], Jeff Dozier[2], Karl Rittger[3], Timbo Stillinger[1], William Kleiber[4], and Robert E. Davis[5]

[1]Earth Research Institute, University of California, Santa Barbara, CA USA 93106
[2]Bren School of Environmental Science and Management, University of California, Santa Barbara, CA USA 93106
[3]Institute of Arctic and Alpine Research, University of Colorado, Boulder, CO 80309
[4]Department of Applied Mathematics, University of Colorado, Boulder, CO 80309
[5]Cold Regions Research and Engineering Laboratory, Hanover, NH USA 03755

Correspondence to: Edward H. Bair (nbair@eri.ucsb.edu)

Abstract

Given the tradeoffs between spatial and temporal resolution, questions about resolution optimality are fundamental to the study of global snow. Answers to these questions will inform future scientific priorities and mission specifications. Heterogeneity of mountain snowpacks drives a need for daily snow cover mapping at the slope scale (≤ 30 m) that is unmet for a variety of scientific users, ranging from hydrologists to the military to wildlife biologists. But finer spatial resolution usually requires coarser temporal or spectral resolution. Thus, no single sensor can meet all these needs. Recently, constellations of satellites and fusion techniques have made noteworthy progress. The efficacy of two such recent advances is examined: 1) a fused MODIS - Landsat product with daily 30 m spatial resolution; and 2) a harmonized Landsat 8 - Sentinel 2A/B (HLS) product with 2-3 day temporal and 30 m spatial resolution. State-of-art spectral unmixing techniques are applied to surface reflectance products from 1 & 2 to create snow cover and albedo maps. Then an energy balance model was run to reconstruct snow water equivalent (SWE). For validation, lidar-based Airborne Snow Observatory SWE estimates were used. Results show that reconstructed SWE forced with 30 m resolution snow cover has lower bias, a measure of basin-wide accuracy, than the baseline case using MODIS (463 m cell size), but higher mean absolute error, a measure of per-pixel accuracy. However, the differences in errors may be within uncertainties from scaling artifacts e.g., basin boundary delineation. Other explanations are 1) the importance of daily acquisitions and 2) the limitations of downscaled forcings for reconstruction. Conclusions are: 1) spectrally unmixed snow cover and snow albedo from MODIS continue to provide accurate forcings for snow models; and 2) finer spatial and temporal resolution through sensor design, fusion techniques, and satellite constellations are the future for Earth observations.

1. Introduction

Mountain snowpacks are challenging for remote sensing because they change rapidly. Moderate resolution sensors such as MODIS and VIIRS image Earth daily, but at resolutions (463 m - 750 m) that cannot resolve slope scale features of interest to a variety of scientific users ranging from hydrologists (Blöschl, 1999), to the military (Vuyovich et al., 2018), to wildlife

biologists (Conner et al., 2018). Finer resolution multispectral sensors such as Landsat 8/9 provide spatial resolutions of 30 m, but at 16-day revisits, during which time the snow cover can change considerably. Because of cloud cover, useable optical

35   imagery with such infrequent revisits can be months apart. Recognizing that no single satellite/instrument can provide fine spatial and temporal resolution, constellations of satellites with coordinated overpass times have emerged. Two examples are the Sentinel 2 A/B and Landsat 8/9 pairs. For optical bands, the Sentinels image Earth every 5 days at 20 m, and Landsats 8/9 image Earth every 8 days at 30 m. The Harmonized Landsat 8/9 Sentinel 2 (HLS) product (Claverie et al., 2018) improves the revisit time to 2-3 days at 30 m spatial resolution.

40   Effects of snow cover estimates at finer resolution have been examined in a few studies, showing a wide range of improvements in errors. In comparing snow cover depletion curves from Landsat MSS (80 m pixels; 16-day repeat) and AVHRR imagery (1100 m pixels; daily repeat), Baumgartner et al. (1987) found that AVHRR tended to overestimate snow cover where it was patchier (lower elevations) and underestimate snow cover where it was more widespread (higher elevations), relative to MSS. They concluded that AVHRR imagery could be used to fill in temporal gaps in depletion curves

45   generated from Landsat MSS. Luce et al. (1998) compared a spatially explicit SWE model at 30 m with single and two point models for a small basin in Idaho. The 30 m model showed significantly lower errors than the single and two point models. Cline et al. (1998) examined the effect of upscaling the spatial resolution of a DEM and snow cover in an energy balance SWE model at a range of resolutions: 30, 90, 250 and 500 m. Positive biases in the coarser resolution estimates arising solely from basin delineation artifacts were reported, thus the authors advise using vector basin outlines (as was done in Section 2.5). When

50   these artifacts were corrected, the SWE volumes at 90 m were overestimates and underestimates at coarser resolutions. Blöschl (1999) examined scaling issues in snow hydrology and shows that pixel sizes of a few m are needed to accurately capture basin-scale SWE. Turpin et al. (2000) examined AVHRR and Landsat TM (30 m resolution; 16-day repeat) derived snow cover maps and report discrepancies, also finding that AVHRR failed to resolve patchy snow compared to TM. Durand et al. (2008) were the first to create a fused MODIS and Landsat product. For the coarse resolution product they used binary snow

55   cover from MODIS (Hall et al., 2002). For the high resolution product they used Landsat 7 ETM+ surface reflectance in a spectral unmixing algorithm (Painter et al., 2003). The authors then used a linear program, constrained to match the ETM+ fractional snow-covered area (fsca) imagery while also matching the daily changes in fsca observed by MODIS. Applying their linear program to the upper Rio Grande, the authors found differences in fsca between the ETM+ fsca, the MODIS fsca, and the fused product. When run through a snow reconstruction model, these differences equated to a 51% reduction in mean

60   absolute error (MAE) and a 49% reduction in bias for SWE using the fused snow cover versus the ETM+ snow cover. Using the same reconstruction model, Molotch and Margulis (2008) report a 23% MAE in SWE using ETM+ snow cover, versus a 50% MAE in SWE using MODIS snow cover, and 89% MAE using AVHRR snow cover. Rittger et al. (2013) examined spectrally unmixed snow cover from ETM+ (similar to the approach in Painter et al., 2009) and several approaches for mapping snow cover from MODIS, including spectral mixture analysis (Painter et al., 2009). They found that ETM+ mapped

65   consistently more patchy snow cover than the MODIS approaches, suggesting fewer false negatives and thus a higher recall statistic. Winstral et al. (2014) examined forcings in a snow energy balance model at a range of spatial resolutions and find

that 100 m spatial resolution is needed to accurately simulate snow melt. Rittger et al. (2021) used a random forest to fuse spectrally unmixed snow cover from MODIS with Landsat 5 and 7 ETM+. The authors' comparisons show sharper snowlines (transition from no snow to fully snow covered) in the Landsat and fused imagery compared to MODIS, again indicating that

70 Landsat may have higher recall than MODIS in this difficult to validate region. In summary, a number of studies have compared coarse and fine resolution snow cover, but only three studies to our knowledge (Cline et al., 1998;Durand et al., 2008;Molotch and Margulis, 2008) have examined the impact of resolution on SWE reconstruction, all finding significant improvements from higher spatial resolution. Since those studies, considerable advances have been made in SWE reconstruction techniques as well as snow cover and albedo mapping, hence the justification for revisiting the effects of spatial

75 and temporal resolution.

2. Approach

Three daily snow cover estimates were used to force a SWE reconstruction model at two spatial resolutions: a baseline at 463 m using MODIS with the Snow Property Inversion from Remote Sensing (SPIReS, Section 2.1, Bair et al., 2021), and two 30 m estimates, one from the Harmonized Landsat-Sentinel (HLS) surface reflectance product (also using SPIReS, Section

80 2.2), the other from Snow Covered Area and Grain Size (SCAG)-Fusion (Section 2.3). The period covered is 1 Jan 2018 to 31 Dec 2020, limited by the intersection of the availability of the SCAG-Fusion and the HLS. The domain is the Tuolumne River Basin above the Hetch Hetchy Reservoir in the Sierra Nevada USA because of the availability of Airborne Snow Observatory (Painter et al., 2016) estimates of SWE for validation. This approach rests on the hypothesis that 1) fsca and 2) snow albedo are the two most important variables in SWE reconstruction (see Section 2.4). The importance of fsca in SWE reconstructions

85 can be traced to several studies (e.g., Durand et al., 2008;Molotch and Margulis, 2008). The importance of snow albedo in SWE reconstructions is shown in Bair et al. (2019).

2.1. SPIReS-MODIS

The baseline case uses MODIS at 463 m daily resolution, although the effective pixel size can be up to 5× as large for off nadir acquisitions (Dozier et al., 2008). The MOD09GA daily surface reflectances (Vermote et al., 2015) are unmixed into

90 fsca and properties used to model albedo (grain size and dust concentration). These estimates are then run through a series of filters including persistence filters for clouds and time-based smoothing/interpolation. Details are provided in Bair et al. (2021).

2.2. SPIReS-HLS

The first daily 30 m snow cover product used also comes from the SPIReS approach applied to the HLS. This is the first snow mapping application, to our knowledge, of HLS data. Thus, we describe the workflow in more detail than SPIReS-

95 MODIS. The Tuolumne River Basin above Hetch Hetchy Reservoir straddles two Sentinel tiles, so HLS version 1.4 multi-band HDF files from both tiles were downloaded (https://hls.gsfc.nasa.gov/). For calendar years 2018-2020, four combinations

of products were downloaded: two tiles (11SKB,11SKC); and two products – S30 (Harmonized Sentinel-2 MSI) and L30 (Harmonized Landsat-8 OLI. We attempted to download the newer HLS version 2.0 from NASA Earthdata Search, but as of this writing, the S30 product for those tiles only extends back to 2020 Sep 23 because of daily limits on the number of Sentinel-
100   2A/B scenes that can be downloaded by NASA from ESA for reprocessing. Seven bands covering visible through shortwave-infrared were used from each sensor: 1-4, 8A, and 11-12 for S30; 1-7 for L30. Mean local solar geometry was obtained from the accompanying header files. The multi-band images were stacked, mosaiced, and cropped to the basin to form a 1119 × 1297 × 7 × 311 4D data structure, with dimensions of rows, columns, bands, and time. Time spacing ranged from around 1 day to 10 days with a mean of 3.5 days (Figure 1). The HLS User's Guide (Masek et al., 2021) states that land observations
105   are available every 2-3 days from the three satellites, but an examination of theoretical revisit times (Li and Roy, 2017) for the constellation at this basin's latitude shows a mean of 3.8 days, with a minimum of less than one day and a maximum of 7.0 days. There are only 4 revisit times greater than 7 days shown in Figure 1; all other observations lie within the theoretical revisit times.
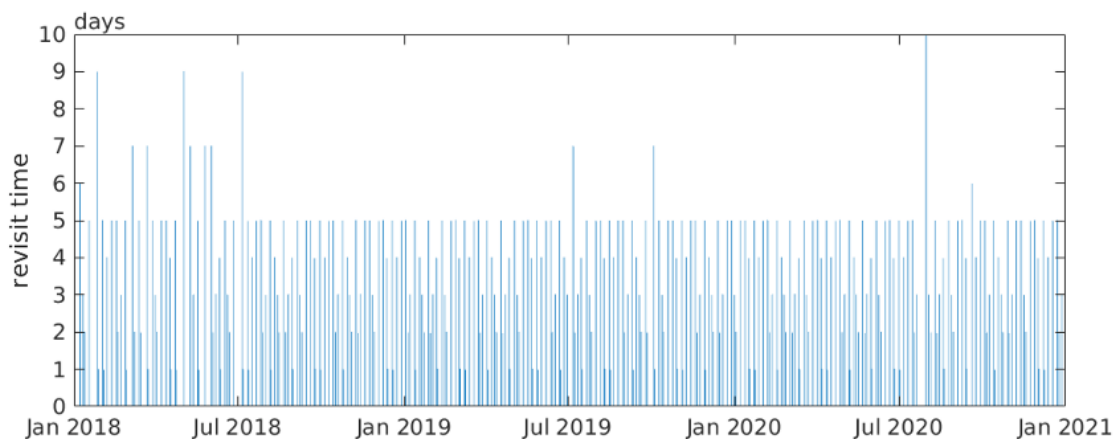
110   Figure 1:

Revisit times covering the Tuolumne River Basin above Hetch Hetchy Reservoir for the HLS S30 and L30 combined.

Red/green/blue band imagery for each day was examined visually. Days with clouds or incomplete spatial coverage over the watershed (many images have large areas with no data) were discarded. After filtering, 156 or about half of the days were kept. The minimum, median, and maximum time spacing between acquisitions after filtering was 1, 5, and 40 days. The
115   SPIReS spectral unmixing approach was then applied to these filtered surface reflectances as described for Landsat 8 OLI in Bair et al. (2021), yielding the variables fsca, snow grain size, and dust concentration. A per-pixel spline interpolation was applied to each of the variables in the time dimension to make them continuous, covering all days from 2018-2020.

2.3. SCAG-Fusion

The second daily 30 m snow cover product used was a MODIS-Landsat fusion, created using two random forests for
120   classification and regression based on previous work (Rittger et al., 2021) but retrained using Landsat 8 OLI data. CFmask
(Foga et al., 2017) cloud cover estimates were used to select the 100 most cloud free Level 2 surface reflectance images (USGS,
2021) for dates spanning Mar 2013 to Mar 2021 (Figure 2). Winter months had less training data than summer months. Six
scenes were manually removed after visual inspection of red/green/blue imagery. Because the initial filtering did not remove
all clouds, a second cloud filtering step using Superpixels and Gabor filtering was used. This second step removed all the
125   clouds, but removed some snow cover as well. These filtered Landsat 8 surface reflectances along with MODIS MOD09GA
surface reflectances were unmixed into fsca and snow surface properties that affect albedo (Painter et al., 2009;Painter et al.,
2012). Note that this SCAG spectral unmixing approach is different than the SPIReS approach. The main differences are that
SPIReS uses an empirical snow-free endmember while SCAG finds the best fit from an endmember library for the snow-free
parts of the pixel. There are other differences in the treatment of light absorbing impurities, filtering, and time-space smoothing
130   (Rittger et al., 2020). For more details and a recent comparison between SPIReS, SCAG, and all other accessible snow mapping
algorithms see Stillinger et al. (2022). Estimates of fsca and snow surface properties that affect albedo i.e., grain size and
visible albedo degradation were used as training data. Physiographic variables, including solar illumination and land
classification were used as predictors. The two-step approach consists of an initial model that classifies pixels into 3 cases: (1)
0%, (2) 100%, or (3) 1-99% fsca. For case (3), a second regression random forest was used to estimate fsca on the 1-99%
135   interval. This two-step classification-regression approach was found to be less biased at predicting 100% snow covered pixels
than using a single-step random forest predicting 0-100% fsca.
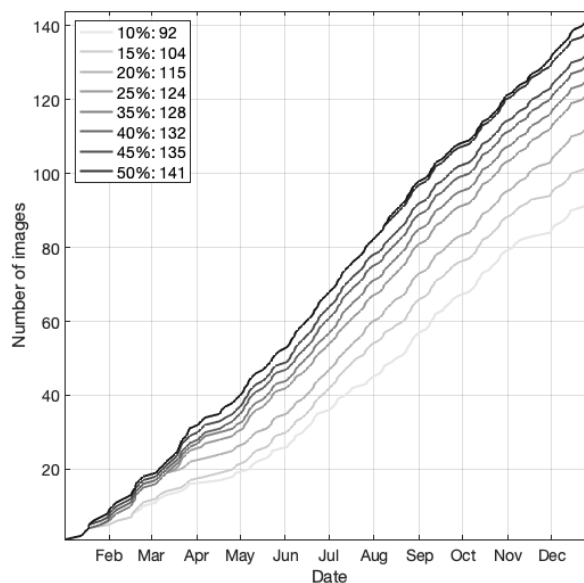
Figure 2:

Cumulative number of images over 8 years acquired from Landsat 8. Lighter to darker lines indicate increasing cloud coverage
140   *from 10-50%. Numbers after the cloud cover percentage in the legend correspond to the total number of images. Images with*
12% or less cloud cover were selected.

2.4. Parallel energy balance

At an hourly timestep, the Parallel Energy Balance model (ParBal) downscales state and flux variables solving for the surface snow energy balance. The computed melt is multiplied by the fsca and summed backward from end-of-melt to peak
145   SWE for each pixel to estimate SWE on the ground throughout the melt season. Details and evaluations of ParBal are covered extensively in previous work (Bair et al., 2016;Rittger et al., 2016;Bair et al., 2018). Evaluations of ParBal (Bair et al., 2016;Bair et al., 2018) forced with snow cover from the MODSCAG approach (Painter et al., 2009;Rittger et al., 2020) show a mean absolute error (MAE) of 22-26% using SWE from ASO for validation. There are two significant changes to ParBal here. 1) U and V wind component forcings use the hourly MERRA-2 (Global Modeling and Assimilation Office (GMAO),
150   2015) data instead of N/GLDAS-2 (Rodell et al., 2004;Xia et al., 2012). Using U & V components with global forcings allows for terrain-based wind downscaling using curvature and slope (Liston et al., 2007), whereas GLDAS only provides wind speed. 2) A new estimate of SWE on the ground, called hybrid SWE, leverages GLDAS SWE (the GLDAS NOAH 3-hour 0.25º v2.1 model was used) and captures the accumulation phase. Previously, ParBal estimates were limited to the ablation phase only. The concept is to identify GLDAS pixels with similar snow cover duration as the fine-scale fsca, find the peak SWE day from
155   those GLDAS pixels, then scale the GLDAS estimates by the ParBal SWE estimate on that peak day. The GLDAS SWE, SWE_{GLDAS}, is extracted for the domain, in this case a bounding box covering the Tuolumne River Basin above Hetch Hetchy Reservoir. Pixels with the same snow cover duration are identified as

$$SWE^*_{GLDAS} = (SWE_{GLDAS} > 0, \text{fsca} > 0) \wedge (SWE_{GLDAS} = 0, \text{fsca} = 0) \tag{1}$$

where the asterisk denotes the selected pixels and fsca is from the fine-scaled product e.g., Section 2.1 - 2.2. Because there can be multiple pixels with matching snow cover duration, the daily mean of SWE^*_{GLDAS} is taken. The maximum value of that
160   daily mean and its index $imax$ are computed. A scaling coefficient c is calculated as

$$c = SWE_{ParBal,imax}/max(\overline{SWE^*_{GLDAS}}) \tag{2}$$

where $SWE_{ParBal,imax}$ is the value of the reconstructed SWE from ParBal (Eq. 2 in Bair et al., 2016) at the time $imax$ and the overbar denotes an average. The following case can arise

$$c = 0, SWE_{ParBal,imax} = 0, (SWE_{GLDAS} > 0) \wedge (\text{fsca} > 0). \tag{3}$$

For example, this case can occur when ParBal models all the mass loss via sublimation. For this case, SWE_{GLDAS} is used when fsca > 0. Otherwise, the hybrid SWE prior to the peak is set at day i as

$$SWE_{hybrid,i} = c \times SWE_{GLDAS,i}, i \leq imax. \tag{4}$$

165   This scaling can cause unrealistic daily increases and decreases in SWE;, thus a smoothing spline is applied. This hybrid SWE has yet to be evaluated throughout the accumulation season, but comparison with the reconstructed SWE during the ASO acquisitions show negligible differences, indicating at least the $imax$ estimate is occurring roughly at the right time of

year since the all of the ASO flights examined here took place during the ablation season (with the exception of 13 Apr 2020, Section 3). ParBal was run with each of the snow cover forcings, holding all other inputs constant.

2.5. Airborne Snow Observatory

ASO 50 m SWE estimates for the Tuolumne River Basin above the Hetch Hetchy Reservoir, which is the most sampled basin by ASO, were downloaded from the National Snow and Ice Data Center for 2018 and 2019 and from ASO Inc. for 2020 (Table 1). The number of acquisitions per year ranged from two (2018) to four (2019) with a total of nine. Accuracy of ASO measurements at the basin scale cannot be estimated directly from data, since there is no better method for validation, but since 2021, ASO has provided basin-wide uncertainty estimates on their reports available on their website (https://www.airbornesnowobservatories.com), mostly based on uncertainty in modeled density, with a small uncertainty in depth. The reported mean basin-wide uncertainty in SWE for ASO flights the entire Tuolumne River Basin for 2021 and 2022 is ±4%, so we assume similar errors in 2018-2020 and use that uncertainty estimate.

Year	Name	Mean SWE, mm
2018	23 Apr	418
	28 May	127
2019	17 Apr	1095
	3 May	840
	13 Jun	441
	5 Jul	111
2020	13 Apr	293
	7 May	191
	21 May	128

Table 1:

Tuolumne River Basin above Hetch Hetchy Reservoir SWE estimates for 2018-2020 for the Airborne Snow Observatory.

2.6. Analysis

The ASO images were resampled from a cell size of 50 m to 2000 m (4× the MODIS resolution) and 120 m (4× the Landsat resolution), using a mean-preserving technique with a weighted resampling covering the image. The ASO images were kept in their native UTM 11N projection. The upscaled cell sizes account for geolocational uncertainty of 1-2 pixels for MODIS and Landsat/Sentinel-2 (Tan et al., 2006;Storey et al., 2016). The ASO dates in Table 1 were extracted for each of the three SWE reconstructions. Then, the matched baseline SPIReS-MODIS images were upscaled from 463 m to 2000 m and reprojected from a sinusoidal projection to UTM 11N. The matched MODIS-Landsat fusion and SPIReS-HLS images were upscaled from 30 m to 120 m but kept in their native UTM 11N projection. Vectors of the Tuolumne River Basin above Hetch

190 Hetchy Reservoir were obtained from ASO Inc. These vectors were then converted into coarse resolution masks of the basin. Water bodies and other areas with no data in either the ASO images or in the SWE reconstructions were removed from the masks. Areas outside of the masks were then set to null values. These common masks were applied to the upscaled SWE reconstruction and ASO images such that areas outside the masks were set to null values. The upscaled ASO images were compared with the upscaled SWE reconstruction images. The following error statistics were computed for a given date: bias

195 as a measure of basin-wide error, relative bias normalized by ASO mean SWE, mean absolute error (MAE) as an unweighted measure of per-pixel error, and relative MAE normalized by ASO mean SWE:

$$\text{bias} = \frac{1}{N}\sum_{j=1}^{N}\text{SWE}_{ParBal,j} - \text{SWE}_{ASO,j} \tag{5}$$

$$\text{relative bias} = \frac{\frac{1}{N}\sum_{j=1}^{N}\text{SWE}_{ParBal,j} - \text{SWE}_{ASO,j}}{\frac{1}{N}\sum_{j=1}^{N}\text{SWE}_{ASO,j}} \tag{6}$$

$$\text{mean absolute error} = \frac{1}{N}\sum_{j=1}^{N}\left|\text{SWE}_{ParBal,j} - \text{SWE}_{ASO,j}\right| \tag{7}$$

$$\text{relative mean absolute error} = \frac{\frac{1}{N}\sum_{j=1}^{N}\left|\text{SWE}_{ParBal,j} - \text{SWE}_{ASO,j}\right|}{\frac{1}{N}\sum_{j=1}^{N}\text{SWE}_{ASO,j}} \tag{8}$$

where N the total number of pixels and j is an individual pixel. Mean values of the four error statistics were also averaged by year. MAE is used instead of Root Mean Squared Error because it evenly weights errors which is preferred when comparing modeled values (Cort and Kenji, 2005) i.e., ParBal to ASO, neither of which directly measure SWE.

200 **2.7. Snow albedo errors**

Errors in snow albedo directly impact the accuracy of reconstructed SWE (Bair et al., 2019). However, for the spectral unmixing approaches used here, the albedo errors are low, evaluated using terrain-corrected measurements from Mammoth Mountain (e.g., Bair et al., 2022), only 23 km from Mount Lyell, the highest point in the Tuolumne River Basin. For example, from water years 2017-2019, the Root Mean Squared Error (RMSE) for MODIS-SPIReS, calculated using the best value for

205 a 3×3 neighborhood around the validation site, is 2.3% with no bias (Table 2). These albedo errors are similar to the accuracy of the HDRF surface reflectance products, evaluated over dark targets (Vermote et al., 2016;Bair et al., 2022). These improvements in remotely sensed snow albedo over previous assessments, showing RMSE values of 4.6 to 4.8% with 0.7-1.3% bias for MODIS (Bair et al., 2019;Bair et al., 2021), come from improved cloud snow discrimination filters and adjustments to thresholds such as the minimum grain size for dirty snow (Section III-J of Bair et al., 2021).

Water year	Bias, %	RMSE, %
2017	-0.8	2.2
2018	-0.3	2.4

2019	1.0	2.4
mean	**0.0**	**2.3**

210   Table 2:

Snow albedo from SPIReS-MODIS validated with terrain-corrected snow albedo from the CUES site on Mammoth Mountain (Bair et al., 2015) taken using an adjustable arm to keep the radiometers 1 m above the snow surface (Bair et al., 2022). A best of 3×3 pixel neighborhood was used to account for geolocational uncertainty.

We are not dismissing errors in albedo, as these remotely-sensed snow albedo errors can lead to 5-11 % MAE for reconstructed

215   SWE (Bair et al., 2019), but without independent measurements of spatially distributed albedo, we lack the validation data for

further error evaluation.

3.   Results and discussion

Basin-wide mean SWE errors are shown in Figure 3a-c and in Table 3. The lower mean MAE, by 10-14% (bold in in Table 3) from SPIReS-MODIS is perhaps the most intriguing result, contradicting the result of previous studies (Section 1)

220   which find that higher spatial resolution estimates of snow cover reduce SWE errors. The reduction of 4-5% relative bias from the two 30 m snow cover forcings compared to MODIS agrees with the previous findings, although the magnitudes of the reductions are smaller than in previous studies (e.g., Durand et al., 2008). To test if the lower MAE from MODIS are resolution artifacts, the SPIReS-HLS and SCAG-Fusion products were also upscaled to 2000 m cell sizes, instead of 120 m. For mean values over all the water years for these upscaled comparisons (Table A1), SPIReS-MODIS still had the lowest relative MAE,

225   but the SCAG-Fusion relative bias dropped to 3% while the SPIReS-HLS relative bias increased to 9%, equal to SPIReS-MODIS. These results suggest that the evaluations are sensitive to the upscaled pixel size, meaning that the differences in errors across the three SWE reconstructions may be within uncertainty bounds introduced by upscaling artifacts such as basin delineation. For example, in the UTM 11N projection, the shapefile obtained from ASO Inc. for the Tuolumne River Basin above Hetch Hetchy Reservoir has an area of 1175 km^2; a raster of the basin at 120 m has an area of 1153 km^2 (-1.8%) while

230   a raster at 2000 m has an area of 1132 km^2 (-3.6%). Even when using vector basin outlines, as suggested by Cline et al. (1998), these artifacts are inherent in the discretization of geospatial data and cannot be eliminated. Other explanations for the lower MAE in SPIReS-MODIS are limitations on downscaling coarse scale reanalysis products (Winstral et al., 2014) e.g., CERES at 1º spatial resolution. Alternatively, the lower MSE may indicate the importance of daily imaging from MODIS compared to the HLS snow cover, which had median gap of 5 days between revisits after filtering for clouds. In contrast, the SCAG-

235   Fusion used daily MODIS snow cover in the prediction and training steps indicating it suffers from errors not related to revisit time.
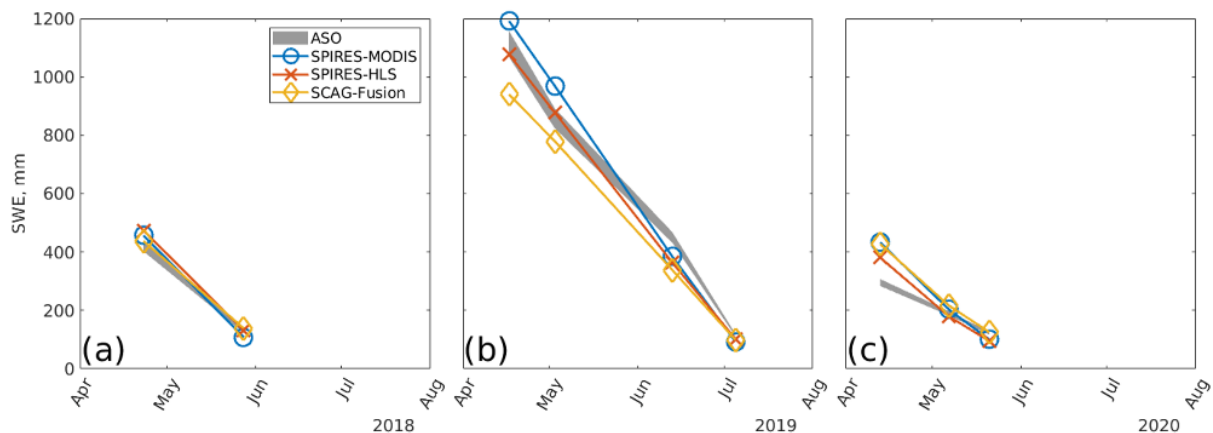
Figure 3:

Basin-side SWE values by date for the three SWE reconstructions (a-c) compared to Airborne Snow Observatory estimates.
240   *Assumed uncertainty in the ASO measurements is ±4% (Section 2.5) and is shaded in gray.*

Name	Year	Bias, mm	Relative Bias, %	MAE, mm	Relative MAE, %
SPIReS-MODIS	2018	9	3	87	32
	2019	26	4	168	26
	2020	43	21	95	47
	mean	**26**	**9**	**117**	**35**
SPIReS-HLS	2018	27	10	135	49
	2019	-24	-4	201	32
	2020	12	6	111	54
	mean	**5**	**4**	**149**	**45**
SCAG-Fusion	2018	13	5	122	44
	2019	-89	-14	264	42
	2020	50	24	123	60
	mean	**-9**	**5**	**170**	**49**

Table 3:

*Error statistics by year for the three SWE reconstructions. Mean values for all years are shown in **bold**. More detailed errors by date are given in the Appendix.*

An example of the SWE modeled by ASO on 4 May 2019 and the three reconstructions is shown in Figure 4. The spatial
245   distribution of the SWE from ASO matches well with all the reconstructions. Differences between the reconstructions can be
seen around Mount Lyell, at the southernmost part of the basin. The ASO SWE shows high variability here, ranging from a
few hundred mm of SWE to over 2000 mm, while the reconstructions model consistently higher amounts of SWE. The
overestimates here are likely related to false-positive classifications for snow. Especially late in the summer, when melt rates are high, these false-positives can lead to substantial overestimates of SWE during reconstruction (Slater et al., 2013). A close

250 examination of the mostly snow-free areas in gray shows that only the SPIReS-HLS reconstructions replicate the small patches of thin snow in this area, likely because the SPIReS-HLS snow cover was not smoothed to the same degree as the SPIReS-MODIS or SCAG-Fusion, which both use heavy smoothing to reduce noise and smearing from MODIS.
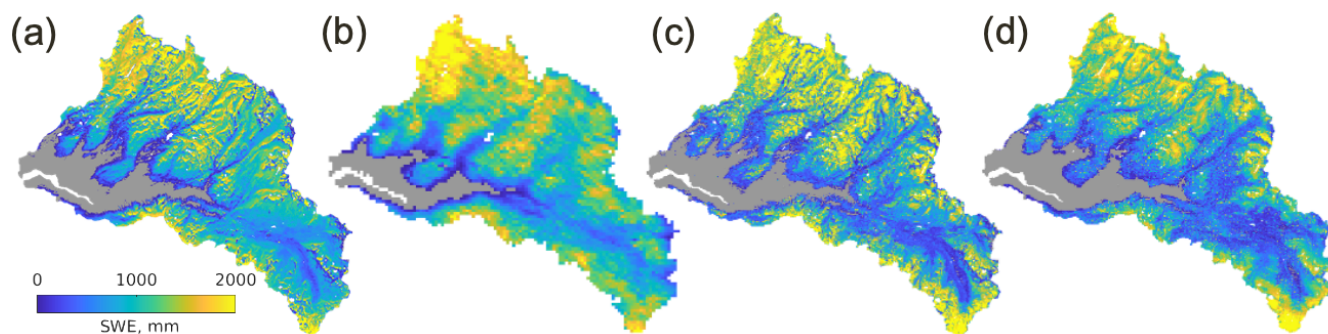
Figure 4:

255 *SWE in the Tuolumne River Basin above Hetch Hetchy Reservoir for 4 May 2019 modeled by the Airborne Snow Observatory (a) along with reconstructions from SPIReS-MODIS (b), SPIReS-HLS (c), and SCAG-Fusion (d).*

Errors are further examined by date (Figure 5 and Table A2). Except for 13 Apr 2020, the bias across all the products is between -20 and 20% (Figure 5a). Figure 6 shows a snow pillow (weighing gauge, California Department of Water Resources station code DAN, elevation 2987 m) and that the ASO flight on 13 Apr 2020 is the only flight in this study that occurred prior

260 to peak SWE. Overestimates of SWE prior to its peak are a limitation of SWE reconstruction. The hybrid SWE method (Section 2.4) extends SWE estimates throughout the year, but the high biases found on this date are not surprising, because snow melt occurred prior to the flight and snow accumulation occurred after the flight. Note the missing data on DAN after 3 May 2018 in Figure 6, but the CUES snow pillow, which is nearby and at a similar elevation (2940 m), shows clear ablation during May 2018.

265 Examination of the per-pixel MAE (Figure 5b) shows that the SPIReS-HLS product has the most consistent values, with the two approaches that used MODIS data (SPIReS-MODIS and SCAG-Fusion), showing more variability, perhaps again due to the smoothing needed for the relatively noisy MODIS data or the fact that SCAG-Fusion was trained using more data outside the test period (March 2013 to December 2017 and January 2021- March 2022) than within it (January 2018 to January 2021).
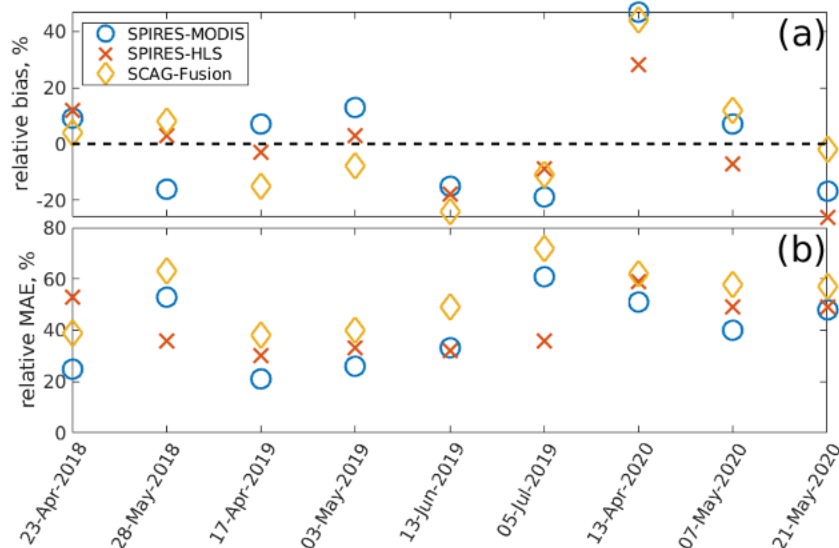
Figure 5:

SWE errors by date for the three SWE reconstructions. The relative bias is show in (a), the relative MAE in (b).
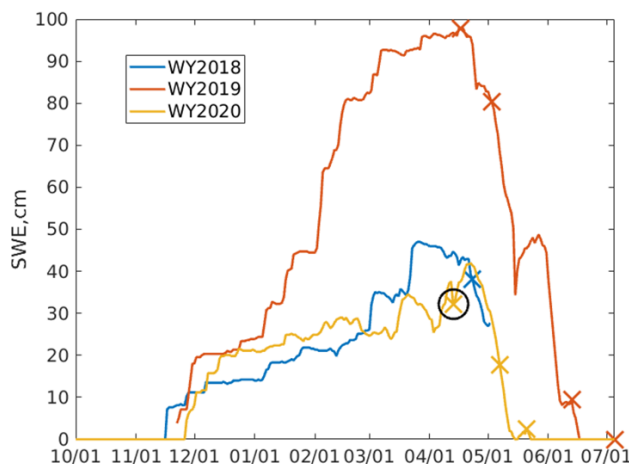
Figure 6:

Snow pillow DAN in the Tuolumne River Basin showing daily SWE. The X markers show the dates of ASO flights. Circled is the 13 Apr 2020 ASO flight, which is the only flight that occurred prior to peak SWE. The pillow was not reporting from 3 May 2018 to 21 Nov 2018, but a nearby snow pillow shows consistent ablation in May 2018.

Stillinger et al. (2022) show that errors in snow cover mapping depend on canopy cover, having to do with how much areal snow is viewable at the pixel scale by a sensor, which affects the accuracy of the SWE reconstructions (Bair et al., 2016). Thus, we examine errors in the SWE reconstructions, binned by canopy cover fraction, for each snow cover forcing. The bin centered at 5% (range: 0 to 9.9%) canopy cover (containing 46-60% of pixels in the basin, Table A3) shows (Figure 7ab)

relatively unbiased errors with MAE values close to the means (Table 3), but SWE biases become positive with increasing canopy cover for SPIReS-MODIS, yet negative for SCAG-Fusion and for SPIReS-HLS (except for the highest canopy fractions which contain only 5% of the basin's pixel, Table A3).
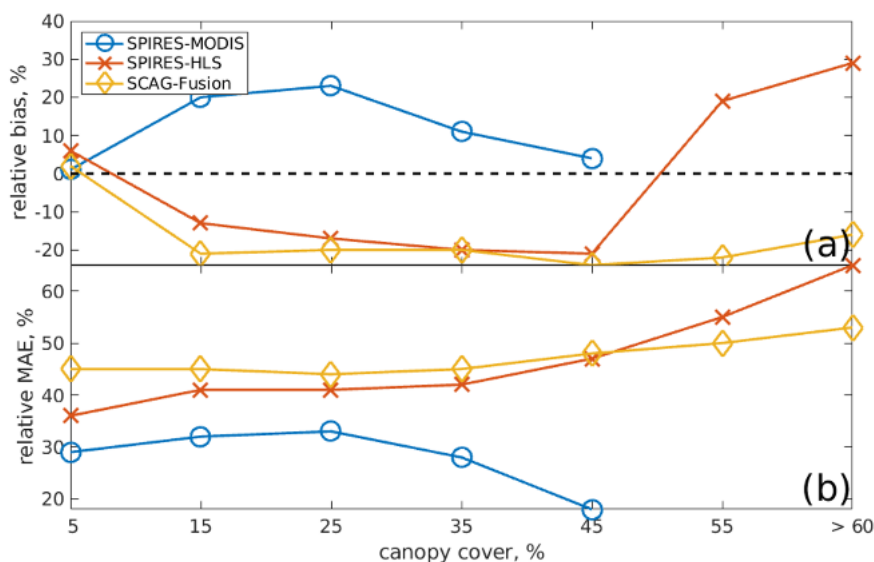
285 Figure 7:

SWE errors for all dates for the three SWE reconstructions binned by canopy cover percent. Labeled are the bin centers. The relative bias is shown in (a), the relative MAE in (b).

The bias and MAE with increasing canopy cover for SPIReS-HLS and SCAG-Fusion SWE reconstructions are similar to errors in fsca from Landsat 8 (Figure 4c, Stillinger et al., 2022). These fsca biases have similar shapes to the SWE biases

290 indicating these fsca errors cause the SWE errors. Conversely, SPIReS-MODIS shows unbiased fsca with increasing canopy cover (Figure 5d, Stillinger et al., 2022), indicating some other source of error in the SPIReS-MODIS SWE reconstructions.

4. Conclusion

Optimal resolution questions are fundamental to the global study of snow and will inform future scientific priorities and mission specifications. Increasing spatial and temporal resolution mark remote sensing achievements with the implicit

295 assumption that higher resolution provides higher accuracy. To test this assumption for snow hydrology, an energy balance SWE reconstruction model was run at two different spatial resolutions using three different snow cover forcings. Contrary to previous work, the baseline case using SPIReS-MODIS, a daily 463 m product, showed a lower MAE–a measure of per-pixel accuracy–compared to SCAG-Fusion and SPIReS-HLS, both with 30 m spatial resolution. The SPIReS-HLS showed the lowest bias, however the differences in the errors between all three products may be within the uncertainty caused by scaling

300 artifacts such as basin boundary delineation. The improved bias with increasing spatial resolution, arguably the most important

measure for water management, is a promising result; however the increased MAE with finer spatial resolution suggests that the daily acquisitions from MODIS provide additional accuracy and/or that there are downscaling limitations with relatively coarse reanalysis data e.g., 10^5 m (1º) downscaled to 30 m. Improvements such as the inclusion of Landsat 9 and version 2.0 of the HLS data may improve some of the errors. Future satellite missions that leverage existing and planned constellations

305   such as Sentinel 2C and Landsat Next will improve revisit times, as gaps between observations are still an issue for the HLS data. In summary, conclusions are: 1) Spectrally unmixed snow cover and snow albedo from MODIS continues to provide accurate forcings for snow models and 2) increased spatial and temporal resolution through sensor design, fusion techniques, and satellite constellations are the future of Earth observations.

310   **Appendix A**

Name	Year	Bias, mm	Relative Bias, %	MAE, mm	Relative MAE, %
SPIReS-MODIS	2018	9	3	87	32
	2019	26	4	168	26
	2020	43	21	95	47
	mean	**26**	**9**	**117**	**35**
SPIReS-HLS	2018	40	15	140	52
	2019	-6	-1	194	31
	2020	26	13	100	50
	mean	**20**	**9**	**145**	**44**
SCAG-Fusion	2018	1	0	90	33
	2019	-108	-17	221	35
	2020	52	26	97	48
	mean	**-18**	**3**	**136**	**39**

Table A1:

Error statistics by date for the three SWE reconstructions, but with all pixels upscaled to 2000 m. The SPIRES-MODIS rows are identical to those in Table 2 and are shown for comparison.

315

Name	Date	Bias, mm	Bias, %	MAE, mm	MAE, %
SPIReS-MODIS	23 Apr 2018	38	9	107	25
	28 May 2018	-20	-16	68	53
	17 Apr 2019	79	7	228	21

	03 May 2019	111	13	223	26
	13 Jun 2019	-66	-15	150	33
	05 Jul 2019	-22	-19	70	61
	13 Apr 2020	137	47	150	51
	07 May 2020	13	7	76	40
	21 May 2020	-21	-17	59	48
SPIReS-HLS	23 Apr 2018	51	12	225	53
	28 May 2018	3	3	46	36
	17 Apr 2019	-32	-3	336	30
	03 May 2019	28	3	284	33
	13 Jun 2019	-79	-18	142	32
	05 Jul 2019	-10	-9	41	36
	13 Apr 2020	84	28	175	59
	07 May 2020	-14	-7	95	49
	21 May 2020	-33	-26	63	49
SCAG-Fusion	23 Apr 2018	15	4	164	39
	28 May 2018	10	8	80	63
	17 Apr 2019	-169	-15	419	38
	03 May 2019	-70	-8	338	40
	13 Jun 2019	-105	-24	216	49
	05 Jul 2019	-13	-11	81	72
	13 Apr 2020	131	44	185	62
	07 May 2020	23	12	111	58
	21 May 2020	-3	-2	74	57

Table A2:

Error statistics by date for the three SWE reconstructions.

Name	Canopy cover, %	Pixels, number	Pixels, %	Bias, mm	Bias, %	MAE, mm	MAE, %
SPIReS-MODIS	5	131	46	7	1	155	29
	15	76	27	68	20	111	32
	25	38	13	57	23	81	33
	35	25	9	23	11	62	28
	45	8	3	8	4	36	18

	55	0	0				
	> 60	0	0				
SPIReS-HLS	5	48230	60	27	6	167	36
	15	8737	11	-45	-13	143	41
	25	6553	8	-59	-17	137	41
	35	6969	9	-64	-20	132	42
	45	5760	7	-59	-21	133	47
	55	2869	4	52	19	152	55
	> 60	962	1	73	29	165	65
SCAG-Fusion	5	48230	60	11	2	212	45
	15	8737	11	-74	-21	156	45
	25	6553	8	-67	-20	148	44
	35	6969	9	-63	-20	141	45
	45	5760	7	-70	-24	137	48
	55	2869	4	-60	-22	136	50
	> 60	962	1	-41	-16	135	53

Table A3:

Error statistics by canopy cover, for all dates, for the three SWE reconstructions.

320 **Code availability**

The codes for ParBal and SPIReS are available on GitHub: https://github.com/edwardbair

The code for SCAG products is not available

Data availability

If accepted, the three snow cover products plus their reconstructions will be placed in a publicly accessible repository such as

325 Dryad (https://datadryad.org). For the review process, the HDF5 datasets of snow cover and reconstructions are hosted on an

FTP site.

SPIReS-MODIS: The snow cover is part of a daily Western US product covering 2001-2021 (Bair and Stillinger, 2022). The

reconstructions are available at ftp://ftp.snow.ucsb.edu/pub/org/snow/products/ParBal/WUS/SPIRESforced

330

SPIReS-HLS: The snow cover and reconstructions are at: ftp://ftp.snow.ucsb.edu/pub/org/snow/products/ParBal

/Tuolumne/spires-hls

SCAG-Fusion: The snow cover and reconstructions are at:

335 ftp://ftp.snow.ucsb.edu/pub/org/snow/products/ParBal/Tuolumne/scag-fusion

Author contribution

According to CRediT taxonomy:

EHB - all 14 contributor roles

340 JD - Conceptualization, writing (review & editing)

KR - Conceptualization, data curation, formal analysis, funding acquisition, methodology, resources, writing (review & editing)

TS - Investigation, writing (review & editing)

WK - Data curation, formal analysis, investigation, methodology, software, supervision

345 RED - Resources, funding acquisition

Competing interests

The first author is a member of The Cryosphere Editorial Board.

Acknowledgements

This research was supported by NASA awards: 80NSSC21K0997, 80NSSC20K1722, 80NSSC20K1349, 80NSSC18K1489,
350 80NSSC21K0620, 80NSSC18K0427, 80NSSC20K1721, 80NSSC22K0703, & 80NSSC22K0929. Other support is from Broad Agency Announcement Program and the Cold Regions Research and Engineering Laboratory (ERDC-CRREL) under Contract No. W913E521C0001.

References

355   Bair, E. H., Dozier, J., Davis, R. E., Colee, M. T., and Claffey, K. J.: CUES – A study site for measuring snowpack energy balance in the Sierra Nevada, Frontiers in Earth Science, 3, 58, 10.3389/feart.2015.00058, 2015.

Bair, E. H., Rittger, K., Davis, R. E., Painter, T. H., and Dozier, J.: Validating reconstruction of snow water equivalent in California's Sierra Nevada using measurements from the NASA Airborne Snow Observatory, Water Resources Research, 52, 8437-8460, 10.1002/2016WR018704, 2016.

360   Bair, E. H., Abreu Calfa, A., Rittger, K., and Dozier, J.: Using machine learning for real-time estimates of snow water equivalent in the watersheds of Afghanistan, The Cryosphere, 12, 1579-1594, 10.5194/tc-12-1579-2018, 2018.

Bair, E. H., Rittger, K., Skiles, S. M., and Dozier, J.: An examination of snow albedo estimates from MODIS and their impact on snow water equivalent reconstruction, Water Resources Research, 55, 7826-7842, 10.1029/2019wr024810, 2019.

365   Bair, E. H., Stillinger, T., and Dozier, J.: Snow Property Inversion from Remote Sensing (SPIReS): A generalized multispectral unmixing approach with examples from MODIS and Landsat 8 OLI, IEEE Transactions on Geoscience and Remote Sensing, 59, 10.1109/TGRS.2020.3040328, 2021.

Bair, E. H., Dozier, J., Stern, C., LeWinter, A., Rittger, K., Savagian, A., Stillinger, T., and Davis, R. E.: Divergence of apparent and intrinsic snow albedo over a season at a sub-alpine site with implications for remote sensing, The
370   Cryosphere, 16, 1765-1778, 10.5194/tc-16-1765-2022, 2022.

Baumgartner, M. F., Seidel, K., and Martinec, J.: Toward Snowmelt Runoff Forecast Based on Multisensor Remote-Sensing Informnation, IEEE Transactions on Geoscience and Remote Sensing, GE-25, 746-750, 10.1109/TGRS.1987.289744, 1987.

Blöschl, G.: Scaling Issues in Snow Hydrology, Hydrological Processes, 13, 2149-2175, 10.1002/(SICI)1099-
375   1085(199910)13:14/15<2149::AID-HYP847>3.0.CO;2-8, 1999.

Claverie, M., Ju, J., Masek, J. G., Dungan, J. L., Vermote, E. F., Roger, J. C., Skakun, S. V., and Justice, C.: The harmonized Landsat and Sentinel-2 surface reflectance data set, Remote Sensing of Environment, 219, 145-161, 10.1016/j.rse.2018.09.002, 2018.

Cline, D., Elder, K., and Bales, R.: Scale effects in a distributed snow water equivalence and snowmelt model for mountain
380   basins, Hydrological Processes, 12, 1527-1536, https://doi.org/10.1002/(SICI)1099-1085(199808/09)12:10/11<1527::AID-HYP678>3.0.CO;2-E, 1998.

Conner, M. M., Stephenson, T. R., German, D. W., Monteith, K. L., Few, A. P., and Bair, E. H.: Survival analysis: Informing recovery of Sierra Nevada bighorn sheep, The Journal of Wildlife Management, 82, 1442-1458, doi:10.1002/jwmg.21490, 2018.

385   Cort, J. W., and Kenji, M.: Advantages of the mean absolute error (MAE) over the root mean square error (RMSE) in assessing average model performance, Climate Research, 30, 79-82, 2005.

Dozier, J., Painter, T. H., Rittger, K., and Frew, J. E.: Time-space continuity of daily maps of fractional snow cover and albedo from MODIS, Advances in Water Resources, 31, 1515-1526, 10.1016/j.advwatres.2008.08.011, 2008.

Durand, M., Molotch, N. P., and Margulis, S. A.: Merging complementary remote sensing datasets in the context of snow
390   water equivalent reconstruction, Remote Sensing of Environment, 112, 1212-1225, 10.1016/j.rse.2007.08.010, 2008.

Foga, S., Scaramuzza, P. L., Guo, S., Zhu, Z., Dilley, R. D., Beckmann, T., Schmidt, G. L., Dwyer, J. L., Joseph Hughes, M., and Laue, B.: Cloud detection algorithm comparison and validation for operational Landsat data products, Remote Sensing of Environment, 194, 379-390, https://doi.org/10.1016/j.rse.2017.03.026, 2017.

Hall, D. K., Riggs, G. A., Salomonson, V. V., DiGirolamo, N. E., and Bayr, K. J.: MODIS snow-cover products, Remote
395   Sensing of Environment, 83, 181-194, 10.1016/S0034-4257(02)00095-0, 2002.

Li, J., and Roy, D. P.: A Global Analysis of Sentinel-2A, Sentinel-2B and Landsat-8 Data Revisit Intervals and Implications for Terrestrial Monitoring, Remote Sensing, 9, 902, 10.3390/rs9090902, 2017.

Liston, G. E., Haehnel, R. B., Sturm, M., Hiemstra, C. A., Berezovskaya, S., and Tabler, R. D.: Instruments and methods: Simulating complex snow distributions in windy environments using SnowTran-3D, Journal of Glaciology, 53, 241-256, 10.3189/172756507782202865, 2007.

Luce, C. H., Tarboton, D. G., and Cooley, K. R.: The influence of the spatial distribution of snow on basin-averaged snowmelt, Hydrological Processes, 12, 1671-1683, https://doi.org/10.1002/(SICI)1099-1085(199808/09)12:10/11<1671::AID-HYP688>3.0.CO;2-N, 1998.

Molotch, N. P., and Margulis, S. A.: Estimating the distribution of snow water equivalent using remotely sensed snow cover data and a spatially distributed snowmelt model: A multi-resolution, multi-sensor comparison, Advances in Water Resources, 31, 1503-1514, 10.1016/j.advwatres.2008.07.017, 2008.

Painter, T. H., Dozier, J., Roberts, D. A., Davis, R. E., and Green, R. O.: Retrieval of subpixel snow-covered area and grain size from imaging spectrometer data, Remote Sensing of Environment, 85, 64-77, 10.1016/S0034-4257(02)00187-6, 2003.

Painter, T. H., Rittger, K., McKenzie, C., Slaughter, P., Davis, R. E., and Dozier, J.: Retrieval of subpixel snow-covered area, grain size, and albedo from MODIS, Remote Sensing of Environment, 113, 868-879, 10.1016/j.rse.2009.01.001, 2009.

Painter, T. H., Bryant, A. C., and Skiles, S. M.: Radiative forcing by light absorbing impurities in snow from MODIS surface reflectance data, Geophysical Research Letters, 39, L17502, 10.1029/2012GL052457, 2012.

Painter, T. H., Berisford, D. F., Boardman, J. W., Bormann, K. J., Deems, J. S., Gehrke, F., Hedrick, A., Joyce, M., Laidlaw, R., Marks, D., Mattmann, C., McGurk, B., Ramirez, P., Richardson, M., Skiles, S. M., Seidel, F. C., and Winstral, A.: The Airborne Snow Observatory: Fusion of scanning lidar, imaging spectrometer, and physically-based modeling for mapping snow water equivalent and snow albedo, Remote Sensing of Environment, 184, 139-152, 10.1016/j.rse.2016.06.018, 2016.

Rittger, K., Painter, T. H., and Dozier, J.: Assessment of methods for mapping snow cover from MODIS, Advances in Water Resources, 51, 367-380, 10.1016/j.advwatres.2012.03.002, 2013.

Rittger, K., Bair, E. H., Kahl, A., and Dozier, J.: Spatial estimates of snow water equivalent from reconstruction, Advances in Water Resources, 94, 345-363, 10.1016/j.advwatres.2016.05.015, 2016.

Rittger, K., Raleigh, M. S., Dozier, J., Hill, A. F., Lutz, J. A., and Painter, T. H.: Canopy Adjustment and Improved Cloud Detection for Remotely Sensed Snow Cover Mapping, Water Resources Research, 56, e2019WR024914, https://doi.org/10.1029/2019WR024914, 2020.

Rittger, K., Krock, M., Kleiber, W., Bair, E. H., Brodzik, M. J., Stephenson, T. R., Rajagopalan, B., Bormann, K. J., and Painter, T. H.: Multi-sensor fusion using random forests for daily fractional snow cover at 30 m, Remote Sensing of Environment, 264, 112608, https://doi.org/10.1016/j.rse.2021.112608, 2021.

Rodell, M., Houser, P. R., Jambor, U., Gottschalck, J., Mitchell, K., Meng, C. J., Arsenault, K., Cosgrove, B., Radakovich, J., Bosilovich, M., Entin, J. K., Walker, J. P., Lohmann, D., and Toll, D.: The Global Land Data Assimilation System, Bulletin of the American Meteorological Society, 85, 381-394, 10.1175/BAMS-85-3-381, 2004.

Slater, A. G., Barrett, A. P., Clark, M. P., Lundquist, J. D., and Raleigh, M. S.: Uncertainty in seasonal snow reconstruction: Relative impacts of model forcing and image availability, Advances in Water Resources, 55, 165-177, 10.1016/j.advwatres.2012.07.006, 2013.

Stillinger, T., Rittger, K., Raleigh, M. S., Michell, A., Davis, R. E., and Bair, E. H.: Landsat, MODIS, and VIIRS snow cover mapping algorithm performance as validated by airborne lidar datasets, The Cryosphere Discuss., 2022, 1-37, 10.5194/tc-2022-159, 2022.

Storey, J., Roy, D. P., Masek, J., Gascon, F., Dwyer, J., and Choate, M.: A note on the temporary misregistration of Landsat-8 Operational Land Imager (OLI) and Sentinel-2 Multi Spectral Instrument (MSI) imagery, Remote Sensing of Environment, 186, 121-122, https://doi.org/10.1016/j.rse.2016.08.025, 2016.

Tan, B., Woodcock, C. E., Hu, J., Zhang, P., Ozdogan, M., Huang, D., Yang, W., Knyazikhin, Y., and Myneni, R. B.: The impact of gridding artifacts on the local spatial properties of MODIS data: Implications for validation, compositing, and band-to-band registration across resolutions, Remote Sensing of Environment, 105, 98-114, 10.1016/j.rse.2006.06.008, 2006.

Turpin, O. C., Caves, R. G., Ferguson, R. I., and Johansson, B.: Verification of simulated snow cover in an Arctic basin using satellite-derived snow-cover maps, Annals of Glaciology, 31, 391-396, 10.3189/172756400781819932, 2000.

Vermote, E., Justice, C., Claverie, M., and Franch, B.: Preliminary analysis of the performance of the Landsat 8/OLI land surface reflectance product, Remote Sensing of Environment, 185, 46-56, https://doi.org/10.1016/j.rse.2016.04.008, 2016.

Vuyovich, C. M., Deeb, E. J., Polashenski, C., Courville, Z., Hiemstra, C. A., Wagner, A. M., Eylander, J. B., and Davis, R. E.: Snow Strategic Science Plan, ERDC/CRREL, Hanover, NH, 91, 2018.

Winstral, A., Marks, D., and Gurney, R.: Assessing the Sensitivities of a Distributed Snow Model to Forcing Data Resolution, J. Hydrometeorol., 15, 1366-1383, 10.1175/jhm-d-13-0169.1, 2014.

Xia, Y., Mitchell, K., Ek, M., Sheffield, J., Cosgrove, B., Wood, E., Luo, L., Alonge, C., Wei, H., Meng, J., Livneh, B., Lettenmaier, D., Koren, V., Duan, Q., Mo, K., Fan, Y., and Mocko, D.: Continental-scale water and energy flux analysis and validation for the North American Land Data Assimilation System project phase 2 (NLDAS-2): 1. Intercomparison and application of model products, Journal of Geophysical Research: Atmospheres, 117, D03109, 10.1029/2011JD016048, 2012.